Journal of the American College of Cardiology
© 2012 by the American College of Cardiology Foundation
Published by Elsevier Inc.

Vol. 60, No. 11, 2012
ISSN 0735-1097/$36.00
http://dx.doi.org/10.1016/j.jacc.2012.02.066

Modeling of Catecholaminergic Polymorphic Ventricular Tachycardia With Patient-Specific Human-Induced Pluripotent Stem Cells

Ilanit Itzhaki, PHD,* Leonid Maizels, BSC,* Irit Huber, PHD,* Amira Gepstein, PHD,* Gil Arbel, MSC,* Oren Caspi, MD, PHD,* Liron Miller, PHD,† Bernard Belhassen, MD,‡ Eyal Nof, MD,† Michael Glikson, MD,† Lior Gepstein, MD, PHD*

Haifa, Tel Hashomer, and Tel-Aviv, Israel

Objectives The goal of this study was to establish a patient-specific human-induced pluripotent stem cells (hiPSCs) model of catecholaminergic polymorphic ventricular tachycardia (CPVT).

Background CPVT is a familial arrhythmogenic syndrome characterized by abnormal calcium (Ca^{2+}) handling, ventricular arrhythmias, and sudden cardiac death.

Methods Dermal fibroblasts were obtained from a CPVT patient due to the M4109R heterozygous point *RYR2* mutation and reprogrammed to generate the CPVT-hiPSCs. The patient-specific hiPSCs were coaxed to differentiate into the cardiac lineage and compared with healthy control hiPSCs-derived cardiomyocytes (hiPSCs-CMs).

Results Intracellular electrophysiological recordings demonstrated the development of delayed afterdepolarizations in 69% of the CPVT-hiPSCs-CMs compared with 11% in healthy control cardiomyocytes. Adrenergic stimulation by isoproterenol (1 μM) or forskolin (5 μM) increased the frequency and magnitude of afterdepolarizations and also led to development of triggered activity in the CPVT-hiPSCs-CMs. In contrast, flecainide (10 μM) and thapsigargin (10 μM) eliminated all afterdepolarizations in these cells. The latter finding suggests an important role for internal Ca^{2+} stores in the pathogenesis of delayed afterdepolarizations. Laser-confocal Ca^{2+} imaging revealed significant whole-cell [Ca^{2+}] transient irregularities (frequent local and large-storage Ca^{2+}-release events, broad and double-humped transients, and triggered activity) in the CPVT cardiomyocytes that worsened with adrenergic stimulation and Ca^{2+} overload and improved with beta-blockers. Store-overload–induced Ca^{2+} release was also identified in the hiPSCs-CMs and the threshold for such events was significantly reduced in the CPVT cells.

Conclusions This study highlights the potential of hiPSCs for studying inherited arrhythmogenic syndromes, in general, and CPVT specifically. As such, it represents a promising paradigm to study disease mechanisms, optimize patient care, and aid in the development of new therapies. (J Am Coll Cardiol 2012;60:990–1000) © 2012 by the American College of Cardiology Foundation

Catecholaminergic polymorphic ventricular tachycardia (CPVT) is a familial arrhythmogenic disorder caused by unstable sarcoplasmic reticulum (SR) calcium (Ca^{2+}) storage leading to exercise- or emotion-induced ventricular tachyarrhythmias and sudden cardiac death (1,2). The majority of CPVT cases are associated with dominant mutations in the cardiac ryanodine receptor gene (*RyR2*) with variable penetrance (CPVT1) (3,4), whereas the minority of cases result from recessive mutations in the cardiac calsequestrin isoform 2 (*CASQ2*) gene (5). Investigation of the mutations giving rise to CPVT provided important insights into the mechanisms underlying this disease and to the processes governing cardiomyocyte Ca^{2+} handling in general (6). Nevertheless, among the hurdles in studying this disease process has been the lack of appropriate human cardiac tissue models and the inability to study patient-specific disease variations.

See page 1001

From *The Sohnis Family Laboratory for Cardiac Electrophysiology and Regenerative Medicine, Rappaport Faculty of Medicine and Research Institute, Technion–Israel Institute of Technology, Haifa, Israel; †AF Laboratory of Leviev Heart Center (Sheba Medical Center), Tel Hashomer, Israel; and the ‡Tel-Aviv Sourasky Medical Center, Tel-Aviv University, Tel-Aviv, Israel. This study was funded by the European Research Council Ideas program (ERC-2010-StG-260830-Cardio-iPS) and by the Nancy and Stephen Grand philanthropic fund. The authors have reported that they have no relationships relevant to the contents of this paper to disclose. The first two authors contributed equally to this work.

Manuscript received October 20, 2011; revised manuscript received January 25, 2012, accepted February 15, 2012.

The development of the groundbreaking human- induced pluripotent stem cells (hiPSCs) technology (7,8) may provide a possible solution to the aforementioned challenges. The iPSCs approach, pioneered by Takahashi and Yamanaka, allows the reprogramming of adult somatic cells into pluripotent stem cells by ectopic expression of a set of transcription factors (9). Subsequent studies showed the robust ability to generate hiPSCs and to coax their differentiation into cardiomyocytes (10,11). More recent proof-of-concept studies demonstrated the ability to establish patient- and disease-specific hiPSCs-derived cardiomyocytes (hiPSCs-CMs) that could recapitulate the abnormal cardiac phenotypes of Leopard and long-QT syndromes (12–14). In the current report, our goal was to establish an hiPSCs model of CPVT. We hypothesized that the generated CPVT-hiPSCs-CMs will recapitulate the disease phenotype in vitro, providing insights into disease mechanisms and offering a unique platform to evaluate patient-specific therapies.

Abbreviations and Acronyms

AP = action potential
CASQ2 = cardiac calsequestrin isoform 2
CPVT = catecholaminergic polymorphic ventricular tachycardia
DADs = delayed afterdepolarizations
EB = embryoid body
hiPSC = human-induced pluripotent stem cell
hiPSCs-CMs = human-induced pluripotent stem cells–derived cardiomyocytes
PCR = polymerase chain reaction
RT-PCR = real-time polymerase chain reaction
RyR2 = ryanodine receptor isoform 2
SOICR = store-overload–induced Ca^{2+} release
SR = sarcoplasmic reticulum

Methods

hiPSCs generation and cardiomyocyte differentiation. The patient-specific hiPSCs clones were generated by retroviral reprogramming of dermal fibroblasts with *Oct-4*, *Sox-2,* and *Klf-4* followed by valproic acid treatment as previously described (13,15). Cardiomyocyte differentiation was induced using the embryoid body (EB) differentiating system. Briefly, undifferentiated hiPSCs were removed from the mouse embryonic fibroblast feeder-layer, dispersed into cell-clumps using collagenase type IV (300 U/ml [Life Technologies Corporation, Grand Island, New York]), cultivated in suspension for 10 days as EBs, and plated on gelatin-coated culture dishes (11).

Immunostainings. Specimens were fixed with 4% paraformaldehyde, permeabilized with 1% Triton, blocked with 5% horse serum, and incubated with primary antibodies targeting: Oct4, Tra1-60 (Santa-Cruz Biotechnology, Santa Cruz, California), Nanog (Peprotech, Rehovot, Israel), SSEA-4 (R&D Systems, Minneapolis, Minnesota), troponin I, ryanodine receptor (Chemicon, Merck Millipore, Billerica, Massachusetts), and sarcomeric alpha actinin (Sigma-Aldrich, St. Louis, Missouri). The preparations were incubated with secondary antibodies and examined using a laser-scanning confocal microscope (Zeiss LSM-510-PASCAL). Alkaline phosphatase staining of hiPSCs colonies was performed using a Sigma detection kit.

Teratoma formation. Undifferentiated hiPSCs were dissociated with collagenase-IV and injected subcutaneously into SCID/beige mice. Tumor samples were collected at 6 to 8 weeks, fixed in 4%-formaldehyde, embedded in paraffin, sectioned, and stained with hematoxylin and eosin.

Genomic sequencing. Genomic DNA was isolated by using the high-pure polymerase chain reaction (PCR) template preparation kit (Roche, Basel, Switzerland). The relevant DNA fragment of the *RYR2* gene was amplified by PCR using 100-ng genomic DNA. Primers are detailed in Online Table 1. PCR products were then sequenced.

Gene expression analysis. RNA was isolated by using the RNeasy Plus Mini Kit (Qiagen Inc., Valencia, California). Reverse transcription into cDNA was conducted with the high-capacity cDNA reverse-transcription kit (Applied Biosystems). Real-time polymerase chain reaction (RT-PCR) studies were performed by using the DreamTaq Master Mix (Ferments Molecular Biology Tools, Thermo Fisher Scientific, Waltham, Massachusetts). Primers are listed in Online Table 1. Each RT-PCR included 2 min at 93°C followed by 27 to 35 cycles of 30 s at 93°C, 60 s at 60°C, and 40 s at 72°C.

RT-PCR studies were conducted in triplicate by using the Fast SYBR Green Master Mix (Applied Biosystems, Life Technologies Corporation). Primers are detailed in Online Table 2. Samples were cycled by using the Fast ABI-7500 sequence detector. Conditions were as follows: 20 s at 95°C followed by 40 cycles of 3 s at 95°C and 30 s at 60°C. Cycle threshold was calculated by using default settings for the real-time sequence detection software (Applied Biosystems).

Whole-cell patch-clamp recordings. Contracting EBs were enzymatically dispersed (1 mg/ml collagenase B [Roche]) and attached to fibronectin-coated glass coverslips. Action potentials (APs) were recorded from spontaneously contracting and quiescent hiPSCs-CMs at 32°C under spontaneous and paced (1 Hz) rhythms. The tyrode solution included (in mmol/l: NaCl 140; KCl 4; $CaCl_2$ 2; $MgCl_2$ 1; HEPES 10; and glucose 5 (pH 7.4; NaOH). The pipette solution contained (in mmol/l): K-aspartate 120; KCl 20; $MgCl_2$ 1; Na_2ATP 4; GTP 0.1; HEPES 10; and glucose 10 (pH 7.2; KOH). APs were recorded in the current-clamp mode with Axopatch 200B, Digidata 1322A, and pClamp 9 (Axon Instruments, Sunnyvale, California).

Microelectrodearray recordings. Microelectrodearray recordings (Multichannels Systems, Reutlingen, Germany) were performed as previously described (11,16). Local activation times were determined at each electrode and used for generation of color-coded activation maps.

Ca^{2+} imaging. Cells were loaded with 5μM fluo-4 fluorescent Ca^{2+} indicator (Molecular Probes, Life Technologies Corporation) to allow recordings of whole-cell $[Ca^{2+}]_i$ transients as previously reported (15). Experiments were

conducted during continuous tyrode perfusion that included (in mmol/l) NaCl 140; KCl 5.4; $CaCl_2$ 1.8; $MgCl_2$ 1; HEPES 10; and glucose 10. $[Ca^{2+}]_i$ imaging was performed by using the Zeiss LSM-700 confocal system. To evaluate for store-overload–induced Ca^{2+} release (SOICR), we used a modification of the method described by Jiang et al. (17,18). In brief, repeated Ca^{2+} imaging from the hiPSCs-CMCs was performed at increasing extracellular $[Ca^{2+}]_o$ concentrations (0.1 to 4 mmol/l) in the presence of tetrodotoxin (10 μM). Tetrodotoxin was added to eliminate AP-dependent Ca^{2+} releases, thereby unmasking only SOICR events.

Statistical analysis. Continuous variables are reported as mean ± SEM. Categorical variables are expressed as frequencies. Categorical differences between groups were evaluated by using the chi-square test. Differences between group means were compared by using the unpaired Student *t* test. These statistical tests were applied to comparisons between the cells obtained from the 2 individuals studied and cannot necessarily be generalized to differences between patient populations. $p < 0.05$ was considered statistically significant.

Results

Derivation of the patient-specific CPVT-hiPSCs. Dermal fibroblasts were obtained from a 30-year-old woman diagnosed with CPVT1. The patient comes from a family with a significant history of sudden cardiac death (including the patient's father, brother, sister, and nephews) (19) and was implanted prophylactically with an implantable cardioverter-defibrillator. An episode of nonsustained ventricular tachycardia was documented during device follow-up and after an epinephrine stress test (Fig. 1A). Genetic workup revealed a heterozygous missense mutation (M4109R) in the RyR2 gene in all affected family members (19).

Several CPVT-hiPSCs clones were generated during reprogramming of the patient's fibroblasts, 2 of which were

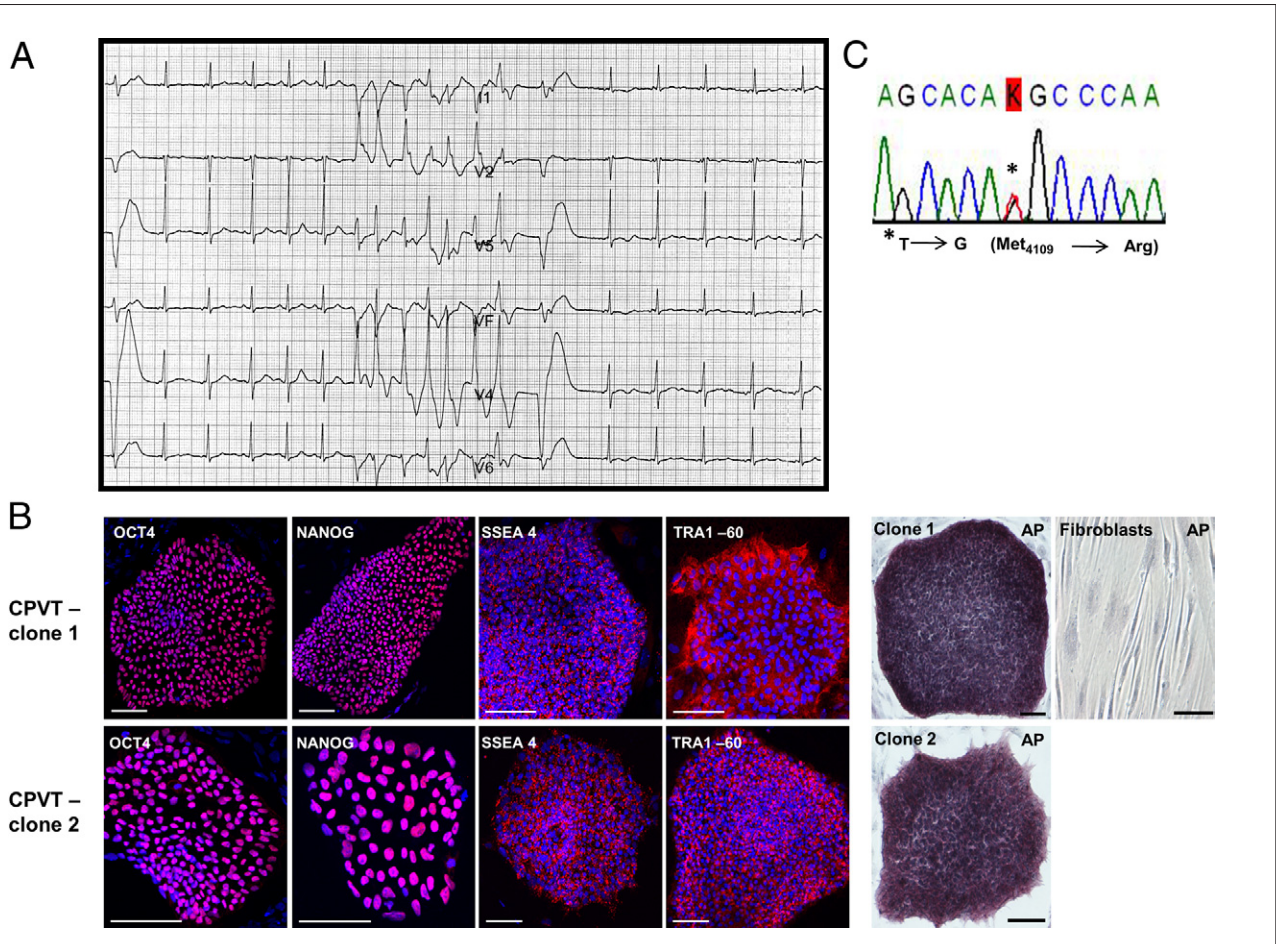

Figure 1 Derivation and Characterization of the CPVT-hiPSCs

(A) Electrocardiogram of the catecholaminergic polymorphic ventricular tachycardia (CPVT) patient showing the development of nonsustained polymorphic ventricular tachycardia during epinephrine testing. **(B)** Immunostaining of undifferentiated CPVT–human-induced pluripotent stem cell (hiPSC) colonies (from 2 clones) for the pluripotent markers OCT4, NANOG, SSEA4, and TRA1-60. Note also the positive staining for alkaline-phosphatase (AP **[right]**). Bars: 100 μm. **(C)** Sequencing of the *RYR2* gene identifying the M4109R heterozygous point mutation in the CPVT-hiPSCs.

propagated and used for cardiomyocyte differentiation and characterization (Fig. 1B). Similar hiPSCs previously created from fibroblasts of a healthy individual (15) served as controls. Importantly, the M4109R mutation was identified in the CPVT-hiPSCs but not in the healthy control cells (Fig. 1C).

The CPVT-hiPSCs colonies exhibited characteristic human embryonic stem cell morphology; stained positively for the pluripotency markers NANOG, OCT4, SSEA-4, and TRA1-60 (Fig. 1B); displayed alkaline phosphatase activity (Fig. 1B [right panel]); and maintained a normal karyotype (data not shown). Pluripotency of the CPVT-hiPSCs was confirmed by the presence of cell-derivatives of all 3 germ-layers in differentiating EBs (Fig. 2A). Note the positive staining for nestin (ectodermal marker), alpha-fetoprotein (endoderm), and desmin (mesoderm) (Fig. 2A). Similarly, injection of undifferentiated CPVT-hiPSCs into SCID/beige mice led to the formation of teratomas, containing advanced tissue derivatives of all 3 germ layers (Fig. 2B). Finally, all clones showed silencing of the 3 retroviral transgenes (Fig. 2C) and reactivation of endogenous pluripotency genes (*OCT4*, *SOX2*, *NANOG*, *FOXD3*, and *REX1*) (Fig. 2D), indicating successful reprogramming.

Cardiomyocyte differentiation. We next used the EB differentiation system to coax the differentiation of the hiPSCs into the cardiac lineage. Both the healthy control and CPVT hiPSCs lines showed similar cardiomyocyte differentiation potential as judged by the number of contracting EBs generated during differentiation (Fig. 3A) and by comparable quantitative expression of cardiac-specific genes by the differentiating cells (Fig. 3B).

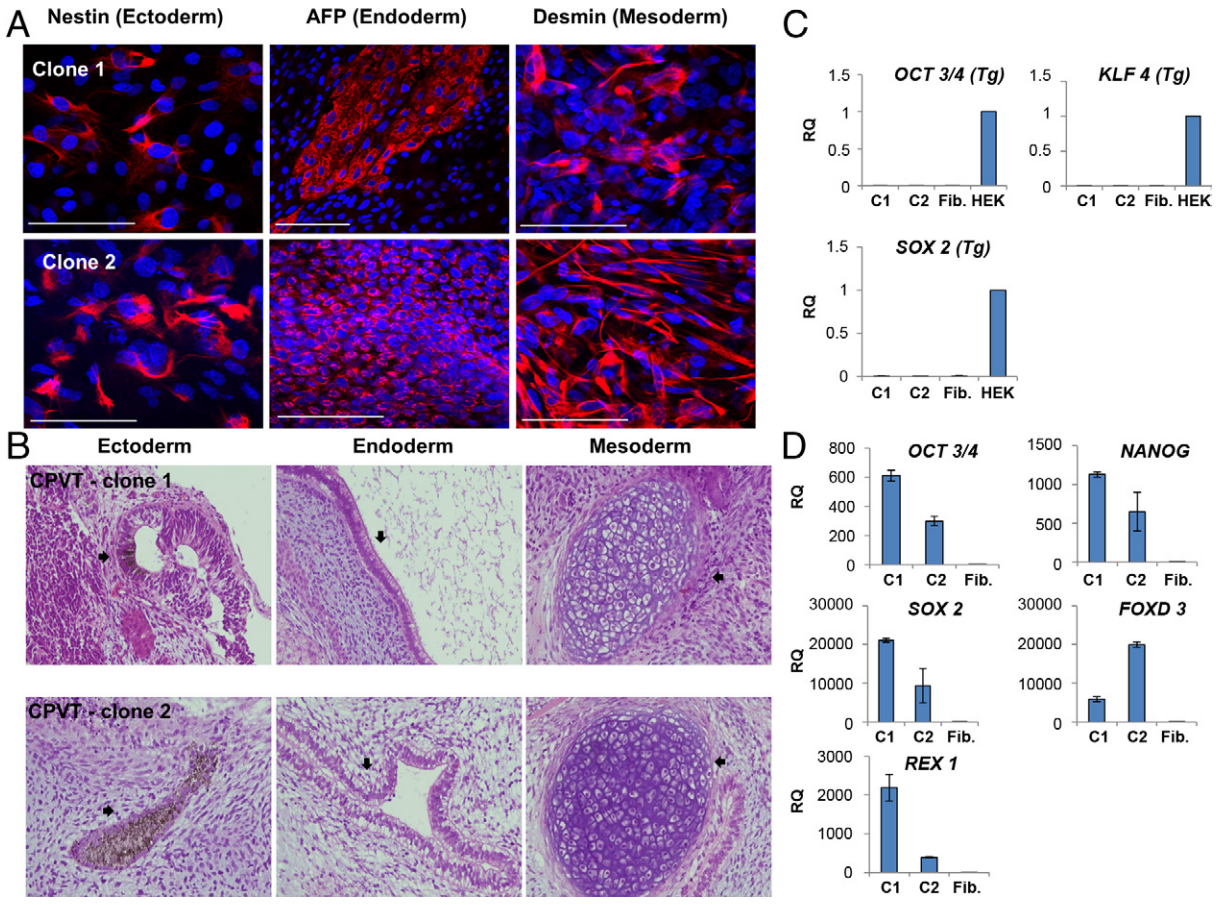

Figure 2 **Characterization of the CPVT-hiPSCs**

(A) Immunostaining of in vitro differentiating embryoid bodies from 2 CPVT-hiPSC clones for nestin (ectoderm), alpha-fetoprotein (AFP; endoderm), and desmin (mesoderm). Scale bars: 100 μm. **(B)** Teratoma formation in SCID/beige mice after injection of undifferentiated CPVT-hiPSCs. Note the presence of pigmented epithelium (ectoderm), columnar-lining epithelium (endoderm), and hyaline cartilage (mesoderm). Scale bars: 100 μm. **(C)** Real-time quantitative polymerase chain reaction (PCR) showing the down-regulation of *OCT3/4*, *KLF4*, and *SOX2* transgenes in the CPVT-hiPSC clones (C1 and C2). Patient's fibroblasts (Fib.) were used as negative controls. Values are normalized to the housekeeping gene *RPL-7* and expressed as mean ± SEM. Expression values (RQ) are relative to HEK293T cells (HEK) transiently transfected with the 3 plasmids to produce reprogramming virions. **(D)** Real-time quantitative PCR evaluating the endogenous levels of the pluripotency genes *OCT 3/4*, *SOX2*, *FOXD3*, *NANOG*, and *REX1* in the CPVT-hiPSC clones. Values are normalized to the housekeeping gene *RPL-7* and expressed as mean ± SEM. Expression values (RQ) are relative to levels in the patient's fibroblasts. Abbreviations as in Figure 1.

JACC Vol. 60, No. 11, 2012
September 11, 2012:990–1000

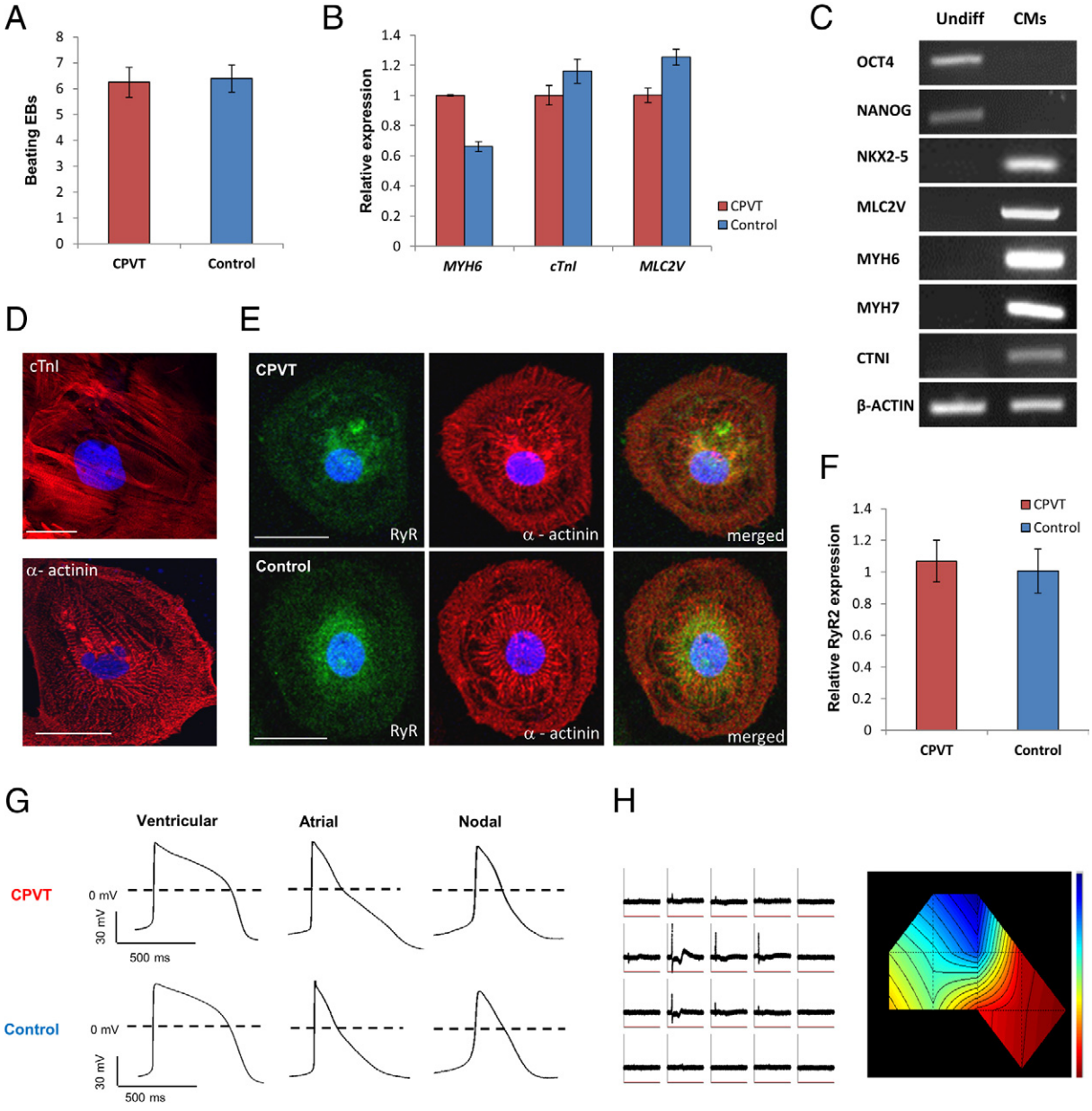

Figure 3 **Phenotypic Characterization of CPVT-hiPSCs-CMs**

(A) Summary of the average number of beating embryoid bodies (EBs)/plate generated during differentiation. Note the similar differentiation capacities of the CPVT and control hiPSCs ($p = 0.86$). **(B)** Real-time quantitative PCR of in vitro differentiating CPVT and healthy control hiPSCs. Note comparable expression levels of cardiac-specific markers (cTnI = cardiac-troponin I; MLC-2V = myosin-light-chain 2-ventricular; *MYH6* = alpha-myosin-heavy-chain). Quantification is relative to levels in the CPVT-hiPSCs-CMCs. Values are normalized to the *RPL-7* gene and displayed as mean ± SEM. **(C)** Semi-quantitative real-time PCR showing expression of cardiac-specific genes by the CPVT-hiPSCs-CMs **(right)**. Undifferentiated (Undiff) hiPSCs (left) express OCT4 and NANOG. **(D)** Immunostainings of CPVT-hiPSCs-CMs for TnI and sarcomeric-alpha-actinin. Bars: 25 μm. **(E)** Immunostainings of CPVT **(top)** and control **(bottom)** hiPSCs-CMs for ryanodine-receptor (RYR) **(green, left)** and sarcomeric-alpha-actinin **(red, middle)**. **Right:** merged image. Bars: 25 μm. **(F)** Real-time quantitative PCR analysis showing equivalent levels of *RyR2* expression between CPVT and healthy control hiPSCs-CMs. Quantification is relative to control cells. Values are normalized to *RPL-7* gene and presented as mean ± SEM. **(G)** Action potential (AP) recordings from the control and CPVT hiPSC-CMCs showing ventricular-like, atrial-like, and nodal-like morphologies. **(H)** Microelectrodearray recordings **(left)** from the CPVT-hiPSC-CMs **(left)** and the resulting color-coded activation map **(right)**. Abbreviations as in Figures 1 and 2.

Gene expression analysis (Fig. 3C) revealed the expression of cardiac-specific transcription factors (*NKX2.5*) and structural genes (*MLC-2V, MYH-6, MYH-7* and *cTnI*) by the CPVT-hiPSCs-CMCs. Similarly, immunostaining studies targeting the sarcomeric proteins troponin I and alpha-actinin confirmed the cardiomyocyte phenotype of these cells (Fig. 3D). These experiments also verified the presence of the major SR Ca^{2+} release channels (RyR2)

in the CPVT-hiPSCs-CMs (Fig. 3E). No differences were noted in RyR2 expression between healthy and diseased hiPSCs-CMs at the mRNA level (Fig. 3F) and also in protein expression and subcellular localization as judged by immunostaining analysis (Fig. 3E).

Intracellular (patch-clamp) and extracellular (multielectrode) electrophysiological recordings established the presence of cardiac-specific APs by the CPVT-hiPSCs-CMs at the cellular level (Fig. 3G) and the development of a functional syncytium at the tissue level (Fig. 3H). Similar to previous reports (10,13), 3 types of AP morphologies were recorded from the CPVT-hiPSCs-CMs (Fig. 3G). The most dominant (57% of cells) was the ventricular-like morphology, with atrial-like (29%), and nodal-like (14%) types being less prevalent.

CPVT-hiPSCs-CMs display afterdepolarizations. Detailed analysis of AP properties (amplitude, upstroke-velocity, durations, and resting membrane potential) revealed no significant differences between the healthy control and CVPT hiPSCs-CMs (Online Table 3). In contrast, marked differences were noted in the cardiomyocytes' arrhythmogenic potential. Hence, clear delayed afterdepolarizations (DADs) developed in most CPVT-hiPSCs-CMs when paced at 0.5 to 1 Hz (Fig. 4A). These DADs were observed in 69% (22 of 32) of the CPVT-hiPSCs-CMs studied (Fig. 4C), with a mean amplitude of 13.0 ± 8.2 mV. In contrast, DADs were only seen in 11% (3 of 28; $p < 0.01$) of the healthy control hiPSCs-CMs (Figs. 4B and 4C) and their amplitude was significantly smaller (5.7 ± 3.9 mV; $p < 0.01$).

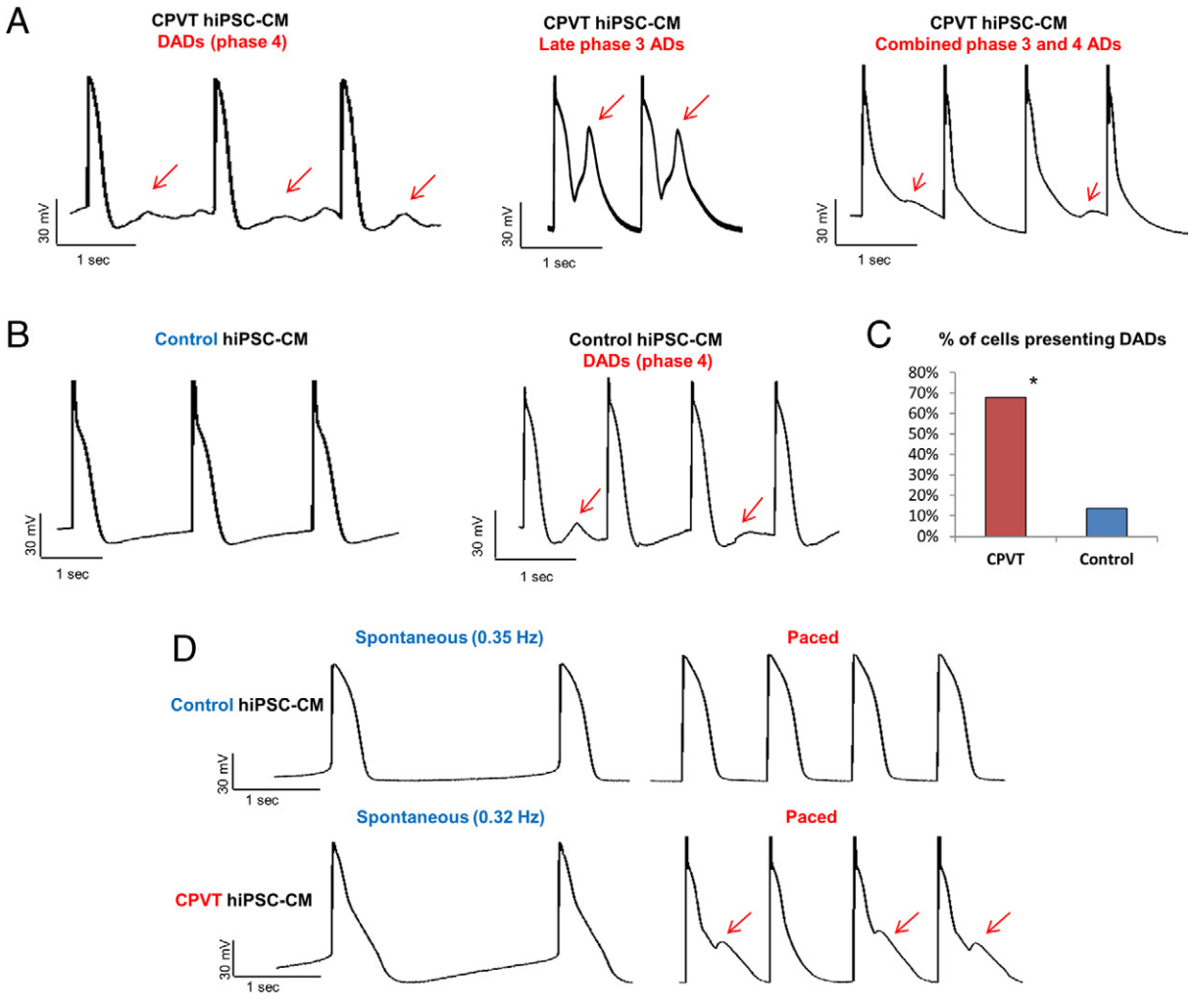

Figure 4 AP Recordings

(A) Action potential (AP) recordings from CPVT-hiPSCs-CMs. Note the development of phase 4 afterdepolarizations **(left)**. Occasionally, afterdepolarizations were also noted during late phase 3, either alone **(middle)** or together with phase 4 afterdepolarizations **(right)**. **(B)** AP recordings from control hiPSCs-CMs. Note that while most cells lacked afterdepolarization (left), small delayed afterdepolarizations (DADs) were noted in some cells **(right)**. **(C)** Summary of the percentage of CPVT and control hiPSCs-CMs displaying afterdepolarizations.*$p < 0.01$. **(D)** AP recordings from control and CPVT-hiPSC-CMs during spontaneous (slow) and more rapid (1-Hz pacing) rates. **Arrows** indicate afterdepolarizations. Abbreviations as in Figure 1.

In the majority of CPVT-hiPSCs-CMs (17 of 22), afterdepolarizations were initiated during phase 4 of the AP (Fig. 4A [left]). In the remaining 5 cells, afterdepolarizations were also noted during late phase 3 (Fig. 4A [middle/right panels]). The severity of the afterdepolarizations in the CPVT-hiPSCs-CMs seemed to correlate with beating frequency (Fig. 4D), and they could be identified both during the stimulation train (Fig. 5A [top]) and immediately after termination of pacing (Fig. 5A [bottom]). Finally, similar percentages of cells displaying afterdepolarizations (62% and 73%) were found in 2 different independently derived CPVT-hiPSCs clones, thus assuring that the aforementioned findings were not related to clonal variations.

Adrenergic stimulation. Because arrhythmias in CPVT are related to exercise or emotional stress, we next evaluated the impact of activation of the adrenergic signaling pathway. Application of forskolin (5 μM), a direct activator of adenylate cyclase, significantly increased the frequency and amplitude of DADs in 83% (5 of 6) of the paced CPVT-hiPSCs-CMs studied and even led to the formation of triggered activity beats in 2 cells (Fig. 5B [top]). We next studied quiescent CPVT-hiPSCs-CMs. Under baseline conditions, with cessation of pacing (Fig. 5A [bottom]), low-amplitude DADs were generated at relatively long coupling intervals. Application of forskolin led to development of multiple DADs in these CPVT-hiPSCs-CMs (exhibiting higher amplitudes and

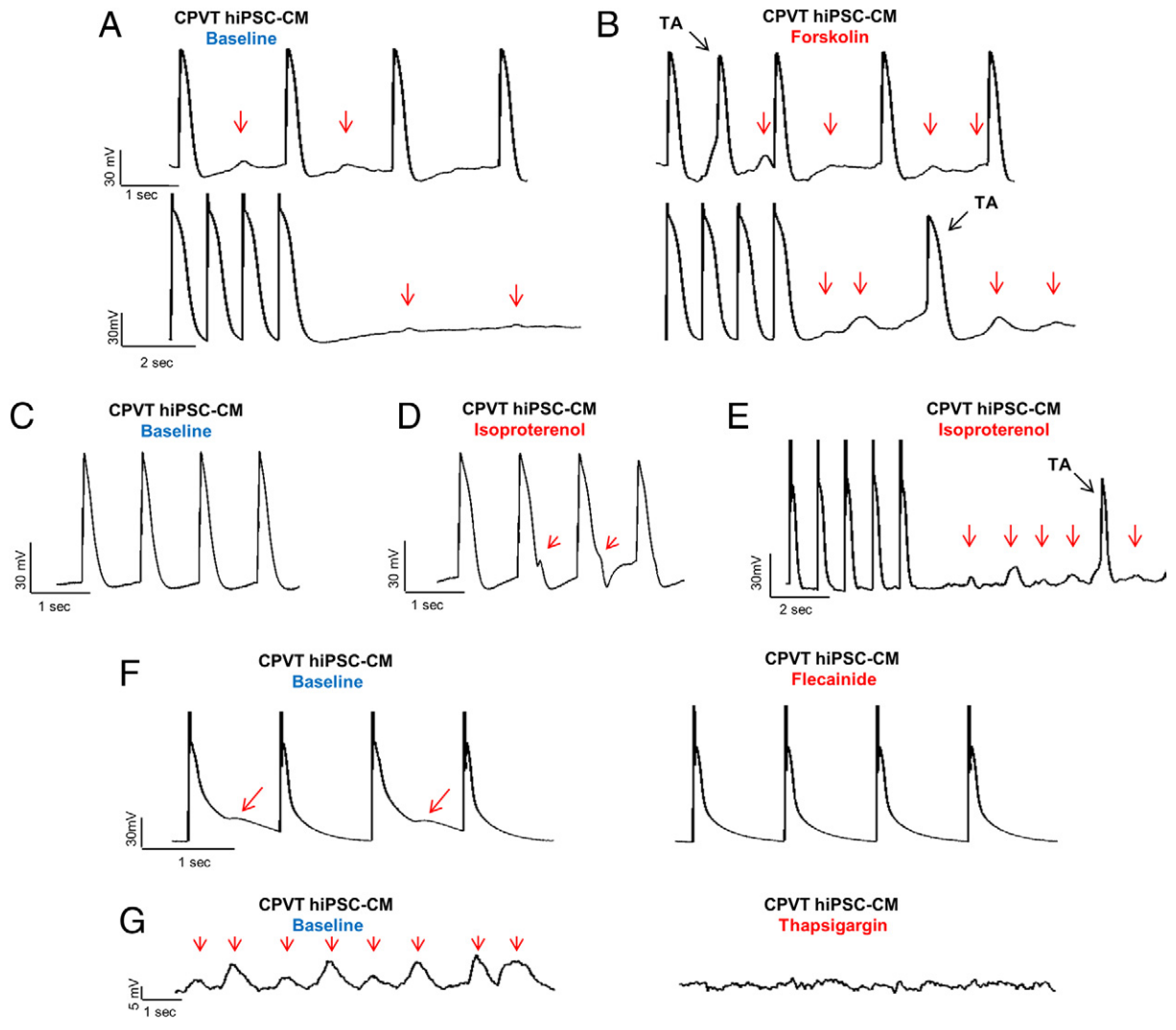

Figure 5 Pharmacological Interventions

AP recordings from the CPVT-hiPSCs-CMs during stimulation **(top)** and after termination of pacing **(bottom)** at **(A)** baseline and **(B)** after application of forskolin 5 μM. Note that forskolin increased the magnitude and frequency of DADs **(arrows)** and also induced triggered activity (TA). **(C to E)** Isoproterenol effects on the CPVT-hiPSCs-CM. Shown are baseline recordings during 1-Hz stimulation **(C)**; isoproterenol led to the development of DADs **(arrows)** and TA during stimulation **(D)** and after termination of pacing **(E)**. **(F)** AP recordings from CPVT-hiPSC-CMs at baseline (afterdepolarizations identified with **arrows, left**) and after flecainide treatment **(right)**. **(G)** Magnification of the postpacing period in the forskolin-treated hiPSCs-CMCs at baseline **(left)** and after treatment with thapsigargin **(right)**. Note the disappearance of DADs. Abbreviations as in Figure 1.

shorter coupling intervals) and even to DAD-mediated triggered activity (Fig. 5B [bottom]).

Application of the beta-agonist isoproterenol also had a proarrhythmic effect in the CPVT-hiPSCs-CMs. Thus, compared with baseline recordings (Fig. 5C), isoproterenol (1 μM) administration resulted in the development of afterdepolarizations in 4 of the 6 cells studied, both during the stimulation train (1 Hz; Fig. 5D), as well as in quiescent cells, after termination of pacing (Fig. 5E). In the latter case, triggered activity was also noted.

Effects of flecainide. A unique advantage of the hiPSCs technology is the potential to screen the effects of therapeutic interventions in a patient-specific manner. To test the feasibility of this concept, we evaluated the effects of flecainide, an antiarrhythmic agent suggested to display antiarrhythmic properties in CPVT (20). As shown in Figure 5F, flecainide 10 μM completely eliminated or significantly decreased afterdepolarizations in all of the patient-specific CPVT-hiPSCs-CMs studied (n = 6).

Role of intracellular Ca^{2+} stores. To verify the role of internal Ca^{2+} stores in the pathogenesis of the observed DADs, we treated the CPVT-hiPSCs-CMs with thapsigargin (10 μM), a specific inhibitor of the sarcoplasmic reticulum calcium ATPase pump. Blocking of Ca^{2+} reuptake into the SR gradually depletes intracellular Ca^{2+} stores. We next evaluated the ability of forskolin-treated cells to develop DADs before and after thapsigargin treatment. As shown in Figure 5G, thapsigargin significantly depressed postpacing afterdepolarizations, indicating the important role of internal Ca^{2+} stores in their formation.

Ca^{2+} imaging. To further evaluate calcium handling, we performed laser-confocal Ca^{2+}-imaging of fluo4-loaded hiPSCs-CMs. As depicted in Figures 6A to 6C, the CPVT-hiPSCs-CMs displayed significant whole-cell $[Ca^{2+}]_i$ transient abnormalities when compared with healthy control cells (Figs. 6D to 6E). These abnormalities were noted in 77% (23 of 30) of the CPVT-hiPSCs-CMs and were manifested by ≥1 of the following: 1) frequent local Ca^{2+} release events interspersed between the regular beats (Fig. 6A); 2) development of large-storage release events (Fig. 6B); and 3) broad double-humped transients (Fig. 6C). In contrast, only 42% (14 of 41) of control cells displayed local Ca^{2+} release events (Fig. 6E), and their amplitudes and durations were lower than those noted in the CPVT-cardiomyocytes. Importantly, none of the control cells developed the more severe whole-cell $[Ca^{2+}]_i$ transient irregularities.

In a similar manner to the electrophysiological recordings, adrenergic stimulation also worsened the degree of Ca^{2+} transient abnormalities in the CPVT-hiPSCs-CMCs. This finding was manifested by the development of new triggered activity events and/or broad double-humped transients in 60% (6 of 10) of the CPVT-hiPSCs-CMs after isoproterenol (1 μM) application (Fig. 6F) and in 75% (6 of 8) of the cells after forskolin (5μM) administration. In contrast, none of the healthy control cells (n = 18 and 13, respectively) displayed such abnormalities following similar interventions (Fig. 6G). Because beta-blockers represent the mainstay treatment for CPVT, we next evaluated their potential effects on the CPVT-hiPSCs-CMs. Application of propranolol (5 μM) reversed the observed abnormalities induced by isoproterenol in 78% (7 of 9) of the cells studied (Fig. 6F).

We next evaluated the effect of Ca^{2+} overload on the degree of Ca^{2+} transient abnormalities in the hiPSCs-CMCs. To this end, the cells were perfused with increasing extracellular Ca^{2+} concentrations ($[Ca^{2+}]_o$). As noted in Figure 6H, this resulted in significant worsening of the Ca^{2+} transient abnormalities (with development of large, wide, and double-humped transients) with elevated $[Ca^{2+}]_o$ in 75% (6 of 8) of the CPVT-hiPSCs-CMs evaluated.

Store-overload-induced Ca^{2+} release (SOICR). It has long been appreciated that SR Ca^{2+} release can also occur in the absence of membrane depolarization through a mechanism referred to as SOICR (6,18). It was also suggested that some RyR2 mutations may markedly increase the occurrence of SOICR (6,18). To evaluate whether SOICR can be modeled by hiPSCs-CMs, we performed repeated Ca^{2+} imaging in tetrodotoxin-treated hiPSCs-CMs at increasing extracellular $[Ca^{2+}]_o$ concentrations (0.1 to 4 mM). As shown in Figure 7A, SOICR events could be identified in both the CPVT and healthy control hiPSC-CMs, with the number of Ca^{2+}-oscillating cells increasing as function of $[Ca^{2+}]_o$ (Fig. 7B). The threshold for generation of SOICR, however, was significantly altered by the M4109R RyR2 mutation. Consequently, the CPVT-hiPSCs-CMs began to develop SOICR at much lower $[Ca^{2+}]_o$ concentrations when compared with healthy control cells (Figs. 7A and 7B).

Discussion

In the current study, we demonstrated the unique potential of hiPSCs for modeling inherited arrhythmogenic syndromes by establishing a patient-specific model of CPVT. By studying cardiomyocytes differentiated from the CPVT-hiPSCs, we were able to: 1) recapitulate the disease phenotype of the CPVT patient by showing the development of DADs in the patient-derived hiPSCs-CMs; 2) identify the role of internal Ca^{2+} stores in the pathogenesis of these afterdepolarizations; 3) reveal the contribution of the beta-adrenergic signaling pathway to these arrhythmias; 4) show the ability of the hiPSCs-CMs to develop SOICR with increasing Ca^{2+} concentrations and the significance of the M4109R RyR2 mutation in altering the threshold for such release events; and 5) demonstrate the potential of patient-specific CPVT-hiPSC-CMs for evaluating candidate drugs such as beta-blockers and flecainide.

Since the realization, more than a decade ago, that mutations in the cardiac ryanodine-receptor gene are responsible for CPVT1 (3,4), much has been learned about the disease pathogenesis. Experimental findings from heterologous expression systems, lipid bilayers, and knock-in

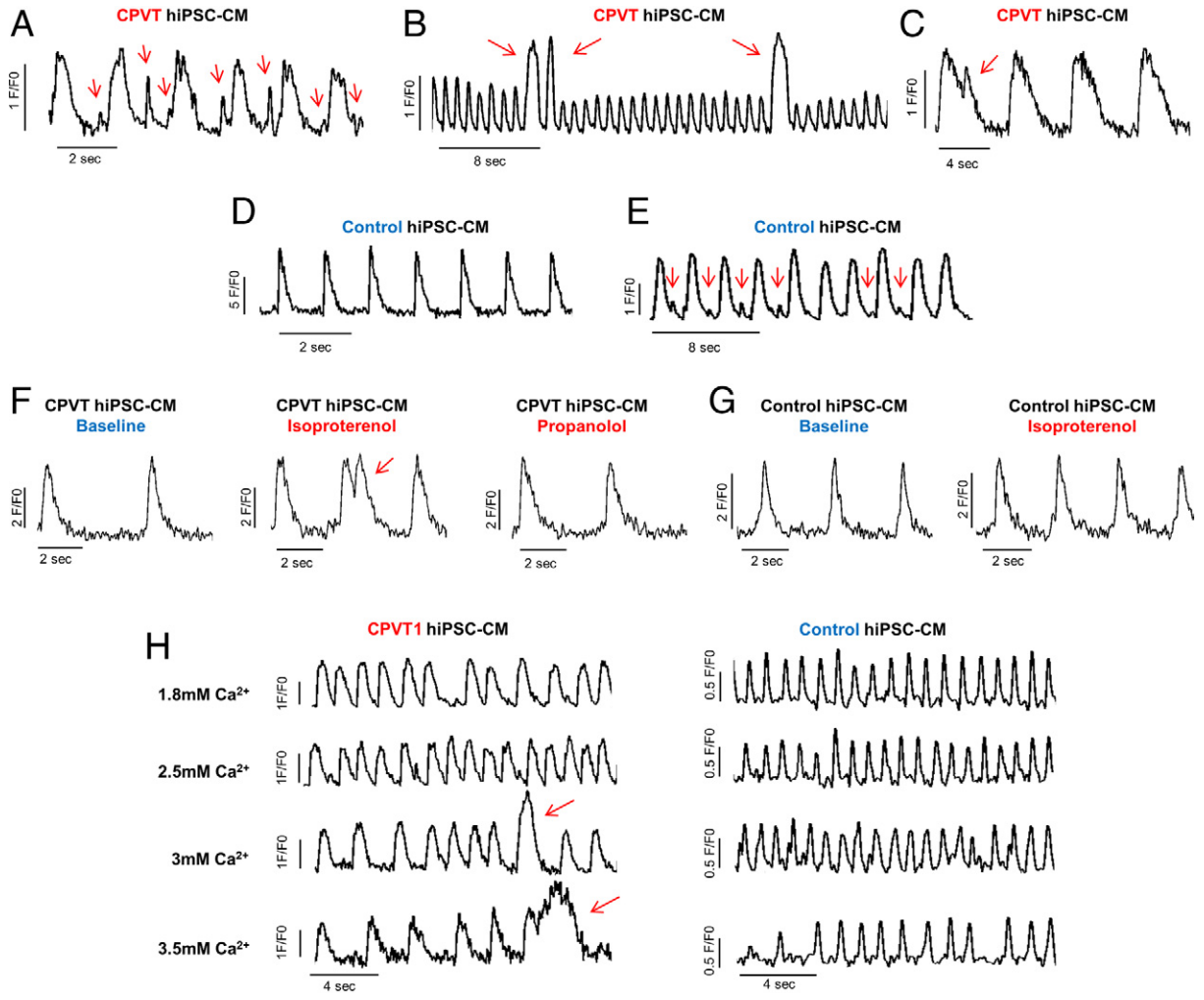

Figure 6 **Whole-Cell $[Ca^{2+}]_i$ Transients in the CPVT and Control hiPSCs-CMCs**

(A to C) Line-scan images showing changes in intracellular Ca^{2+} in fluo-4 loaded CPVT-hiPSCs-CMs. **(A)** Note the development of significant whole-cell $[Ca^{2+}]_i$ transient irregularities manifested as frequent local Ca^{2+} release events **(arrows)**; **(B)** development of large store-release Ca^{2+} waves; and **(C)** broad double-humped transients. **(D, E)** Whole-cell $[Ca^{2+}]_i$ transients in control hiPSCs-CMs. Although most cells lacked significant abnormalities **(D)**, some cells displayed small-amplitude local Ca^{2+} release events **(arrows, E)**. **(F)** Worsening of Ca^{2+}-handling abnormalities in the isoproterenol-treated (1 μM) CPVT-hiPSCs-CMs, manifested by the development of double-humped $[Ca^{2+}]_i$ transients **(middle)**. Propranolol (5 μM) application reversed these abnormalities **(right)**. **(G)** Isoproterenol did not cause irregularities in control hiPSCs-CMs. **(H)** Effect of extracellular $[Ca^{2+}]_o$ concentrations on whole-cell $[Ca^{2+}]_i$ transients recorded from CPVT **(left)** and control **(right)** hiPSCs-CMCs. Note the development of broad and double-humped $[Ca^{2+}]_i$ transients (arrows) in the CPVT-hiPSCs-CMs with higher $[Ca^{2+}]_o$ concentrations. Abbreviations as in Figure 1.

and knockout mice models suggest that the basic mechanism underlying development of arrhythmias in this disorder involves a diastolic Ca^{+2} leak from the mutant RyR2 (6). This may lead to development of DADs through activation of the membrane Na^+/Ca^{2+} exchanger, which can eventually result in triggered activity; the pivotal arrhythmogenic mechanism in CPVT.

One of the challenges in confirming such a mechanism also clinically was the inability to directly study human cardiomyocytes from patients with CPVT. The advent of the hiPSCs technology may solve this cell-sourcing problem. This unique "disease-in-a-dish" concept is based on the capacity to derive isogenic hiPSCs from an affected individual and to coax their differentiation into the desired cell lineage (cardiomyocytes), thus portraying the patient-specific disease phenotype.

We have previously shown that hiPSCs-CMs express the necessary functional components associated with Ca^{2+} handling (15). This was demonstrated by development of spontaneous whole-cell $[Ca^{2+}]_i$ transients in the hiPSCs-CMs, which were dependent on both sarcolemmal Ca^{2+} entry via L-type Ca^{2+} channels and intracellular store Ca^{2+} release (15).

Here, using hiPSCs-CMs derived from a CPVT patient, we provide proof-of-concept evidence that the mechanism thought to underlie arrhythmogenicity in CPVT is also

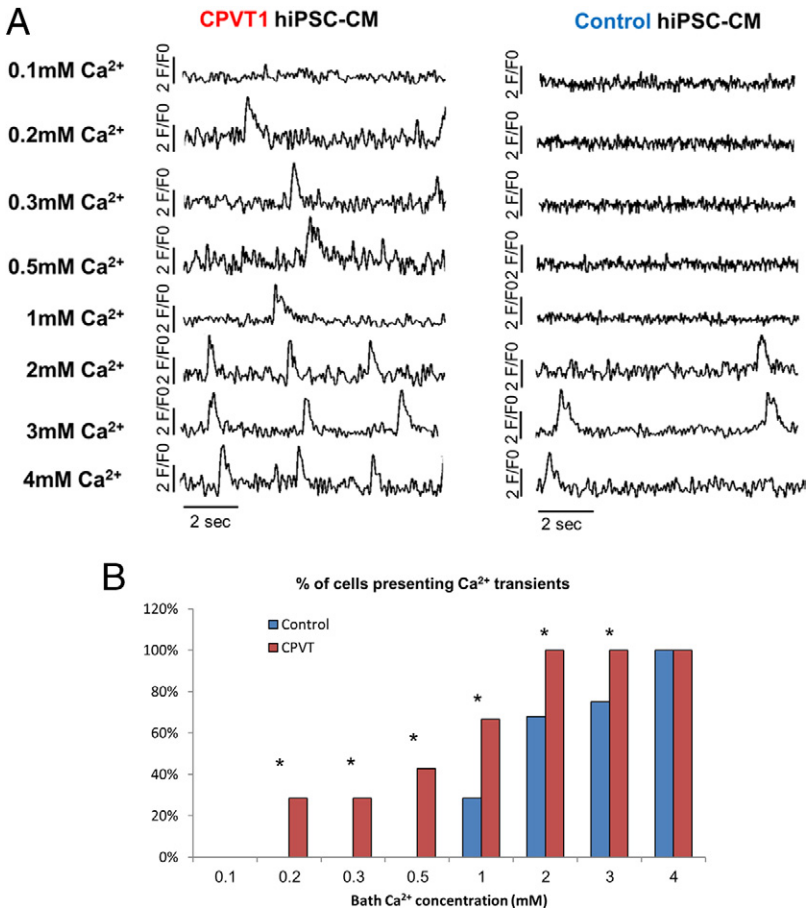

Figure 7 **SOICR in the CPVT hiPSCs-CMs**

(A) Development of store-overload–induced calcium release (SOICR) events in CPVT **(left)** and control **(right)** tetrodotoxin-treated hiPSCs-CMs at different $[Ca^{2+}]_o$ concentrations. Note the development of SOICR events at much lower $[Ca^{2+}]_o$ concentrations in the CPVT cardiomyocytes. **(B)** Percentage of healthy control **(blue)** and CPVT **(red)** hiPSCs-CMs displaying Ca^{2+} oscillations at increasing $[Ca^{2+}]_o$ concentrations. Note the reduced threshold for generating SOICR in the CPVT cells. *$p < 0.05$ when the frequency of Ca^{2+}-oscillating cells is compared between the CPVT and control cells at each concentration. Abbreviations as in Figure 1.

valid in the patient-specific cardiomyocytes. This was shown by the development of DADs in most CPVT-hiPSCs-CMs that became even more prominent after activation of the beta-adrenergic signaling pathway and could eventually give rise to triggered activity.

We next evaluated the role of intracellular Ca^{2+} stores in the formation of these DADs. By depleting internal Ca^{2+} stores with thapsigargin, we were able to suppress afterdepolarizations in the CPVT-hiPSCs-CMs, thus confirming the crucial role of these stores in DADs' pathogenesis. Moreover, in a similar manner to the electrophysiological recordings, laser-confocal Ca^{2+} imaging demonstrated significant Ca^{2+}-handling irregularities in the CPVT-hiPSCs-CMs. These abnormalities, ranging from an increase in the incidence and magnitude of local Ca^{2+} release events to more severe global whole-cell Ca^{2+} irregularities and arrhythmogenesis, worsened with beta-adrenergic stimulation and Ca^{2+} overload.

It is believed that the diastolic Ca^{2+} wave that underlies the generation of DADs occurs when the SR Ca^{2+} content exceeds a threshold level. The mechanism for such a depolarization-independent SR Ca^{2+} release was termed SOICR (6,18), and this process was implicated in the arrhythmogenesis associated with intracellular Ca^{2+} overload, such as during digitalis intoxication. It was also suggested, in both heterologous expression systems (18,21) and in cardiomyocytes derived from a mouse model of CPVT (22), that several RyR2 mutations may markedly reduce the SR Ca^{2+} threshold required for SOICR. In the current study, we demonstrated the ability of the hiPSCs-CMs to recapitulate the SOICR phenomenon with the number of Ca^{2+}-oscillating cells increasing with elevated Ca^{2+} concentrations. We also found that the M4109R RyR2 mutation decreases the threshold for such events, with SOICR occurring in the CPVT-hiPSCs-CMs at much lower Ca^{2+} concentrations then in healthy control cells.

Finally, feasibility studies were performed to demonstrate the potential of the CPVT-hiPSCs-CMs model for drug screening. These studies revealed that beta-blockers, which have been the mainstay treatment for CPVT, may also be beneficial in the patient-specific hiPSCs-CMs by reversing the Ca^{2+}-handling irregularities observed after adrenergic stimulation. In addition to beta-blockers, potential new antiarrhythmic strategies for CPVT include agents targeting the abnormal diastolic Ca^{2+} leak (e.g., RyR2 stabilizers) (23) or those targeting the ionic mechanisms responsible for the generation of triggered activity (6). Flecainide was recently shown to possess antiarrhythmic properties in CPVT (20) through either a stabilizing effect on RyR2 (decreasing its opening probability) (20,24) or by increasing the threshold for triggered activity (through its Na^{+}-channel blocking activity) (25). Although the current study was not designed to shed additional light on the specific antiarrhythmic mechanism of flecainide, it did reveal its ability to eliminate afterdepolarizations and triggered activity in the patient-derived hiPSCs-CMs. In addition, because this work involved a single CPVT patient, future studies will have to expand the results of this study to larger cohorts of patients.

Taken together, our data demonstrate the unique potential of hiPSCs-CMs for modeling CPVT. Using this approach, the disease phenotype presented by the patient at bedside could be readily recognized in the patient-derived cells in vitro as an anomalous electrophysiological signature. Importantly, this study also provided insights into arrhythmia mechanisms in this syndrome and highlighted the potential of the hiPSCs strategy for screening the effects of potential disease aggravators (adrenergic stimulation) and customized treatment options (beta-blockers and flecainide).

Acknowledgments

The authors thank Dr. Doron Aronson for his statistical advice and Dr. Edith Suss-Toby for her help in the imaging studies.

Reprint requests and correspondence: Dr. Lior Gepstein, Rappaport Institute, Technion–Israel Institute of Technology, POB 9649, Haifa 31096, Israel. E-mail: mdlior@techunix.technion.ac.il.

REFERENCES

1. Hayashi M, Denjoy I, Extramiana F, et al. Incidence and risk factors of arrhythmic events in catecholaminergic polymorphic ventricular tachycardia. Circulation 2009;119:2426–34.
2. Leenhardt A, Lucet V, Denjoy I, Grau F, Ngoc DD, Coumel P. Catecholaminergic polymorphic ventricular tachycardia in children. A 7-year follow-up of 21 patients. Circulation 1995;91:1512–9.
3. Laitinen PJ, Brown KM, Piippo K, et al. Mutations of the cardiac ryanodine receptor (RyR2) gene in familial polymorphic ventricular tachycardia. Circulation 2001;103:485–90.
4. Priori SG, Napolitano C, Tiso N, et al. Mutations in the cardiac ryanodine receptor gene (hRyR2) underlie catecholaminergic polymorphic ventricular tachycardia. Circulation 2001;103:196–200.
5. Lahat H, Pras E, Olender T, et al. A missense mutation in a highly conserved region of CASQ2 is associated with autosomal recessive catecholamine-induced polymorphic ventricular tachycardia in Bedouin families from Israel. Am J Hum Genet 2001;69:1378–84.
6. Priori SG, Chen SR. Inherited dysfunction of sarcoplasmic reticulum Ca2+ handling and arrhythmogenesis. Circ Res 2011;108:871–83.
7. Takahashi K, Tanabe K, Ohnuki M, et al. Induction of pluripotent stem cells from adult human fibroblasts by defined factors. Cell 2007;131:861–72.
8. Yu J, Vodyanik MA, Smuga-Otto K, et al. Induced pluripotent stem cell lines derived from human somatic cells. Science 2007;318:1917–20.
9. Takahashi K, Yamanaka S. Induction of pluripotent stem cells from mouse embryonic and adult fibroblast cultures by defined factors. Cell 2006;126:663–76.
10. Zhang J, Wilson GF, Soerens AG, et al. Functional cardiomyocytes derived from human induced pluripotent stem cells. Circ Res 2009;104:e30–41.
11. Zwi L, Caspi O, Arbel G, et al. Cardiomyocyte differentiation of human induced pluripotent stem cells. Circulation 2009;120:1513–23.
12. Carvajal-Vergara X, Sevilla A, D'Souza SL, et al. Patient-specific induced pluripotent stem-cell-derived models of LEOPARD syndrome. Nature 2010;465:808–12.
13. Itzhaki I, Maizels L, Huber I, et al. Modelling the long QT syndrome with induced pluripotent stem cells. Nature 2011;471:225–9.
14. Moretti A, Bellin M, Welling A, et al. Patient-specific induced pluripotent stem-cell models for long-QT syndrome. N Engl J Med 2010;363:1397–409.
15. Itzhaki I, Rapoport S, Huber I, et al. Calcium handling in human induced pluripotent stem cell derived cardiomyocytes. PLoS One 2011;6:e18037.
16. Kehat I, Gepstein A, Spira A, Itskovitz-Eldor J, Gepstein L. High-resolution electrophysiological assessment of human embryonic stem cell-derived cardiomyocytes: a novel in vitro model for the study of conduction. Circ Res 2002;91:659–61.
17. Jiang D, Chen W, Wang R, Zhang L, Chen SR. Loss of luminal Ca2+ activation in the cardiac ryanodine receptor is associated with ventricular fibrillation and sudden death. Proc Natl Acad Sci U S A 2007;104:18309–14.
18. Jiang D, Xiao B, Yang D, et al. RyR2 mutations linked to ventricular tachycardia and sudden death reduce the threshold for store-overload-induced Ca2+ release (SOICR). Proc Natl Acad Sci U S A 2004;101:13062–7.
19. Nof E, Belhassen B, Arad M, et al. Postpacing abnormal repolarization in catecholaminergic polymorphic ventricular tachycardia associated with a mutation in the cardiac ryanodine receptor gene. Heart Rhythm 2011;8:1546–52.
20. Watanabe H, Chopra N, Laver D, et al. Flecainide prevents catecholaminergic polymorphic ventricular tachycardia in mice and humans. Nat Med 2009;15:380–3.
21. Jones PP, Jiang D, Bolstad J, et al. Endoplasmic reticulum Ca2+ measurements reveal that the cardiac ryanodine receptor mutations linked to cardiac arrhythmia and sudden death alter the threshold for store-overload-induced Ca2+ release. Biochem J 2008;412:171–8.
22. Kashimura T, Briston SJ, Trafford AW, et al. In the RyR2(R4496C) mouse model of CPVT, beta-adrenergic stimulation induces Ca waves by increasing SR Ca content and not by decreasing the threshold for Ca waves. Circ Res 2010;107:1483–9.
23. Andersson DC, Marks AR. Fixing ryanodine receptor Ca leak—a novel therapeutic strategy for contractile failure in heart and skeletal muscle. Drug Discov today Disease Mech 2010;7:e151–7.
24. Hilliard FA, Steele DS, Laver D, et al. Flecainide inhibits arrhythmogenic Ca2+ waves by open state block of ryanodine receptor Ca2+ release channels and reduction of Ca2+ spark mass. J Mol Cell Cardiol 2010;48:293–301.
25. Liu N, Denegri M, Ruan Y, et al. Flecainide exerts an antiarrhythmic effect in a mouse model of catecholaminergic polymorphic ventricular tachycardia by increasing the threshold for triggered activity. Circ Res 2011;109:291–5.

Key Words: arrhythmia ■ genetics ■ ryanodine receptor ■ stem cells.

APPENDIX

For supplementary tables, please see the online version of this article.